



## Article

**Cite this article:** Shoemaker IM, Kusenko A, Kuipers Munneke P, Romero-Wolf A, Schroeder DM, Siebert MJ (2020). Reflections on the anomalous ANITA events: the Antarctic subsurface as a possible explanation. *Annals of Glaciology* **61**(81), 92–98. <https://doi.org/10.1017/aog.2020.19>

Received: 21 August 2019  
Revised: 29 March 2020  
Accepted: 30 March 2020  
First published online: 24 April 2020






**Key words:**

Antarctic glaciology; Ice physics; Snow physics

**Author for correspondence:**

Ian Shoemaker,  
E-mail: [shoemaker@vt.edu](mailto:shoemaker@vt.edu)

# Reflections on the anomalous ANITA events: the Antarctic subsurface as a possible explanation

Ian M. Shoemaker<sup>1</sup> , Alexander Kusenko<sup>2,3</sup>, Peter Kuipers Munneke<sup>4</sup> , Andrew Romero-Wolf<sup>5</sup> , Dustin M. Schroeder<sup>6</sup>  and Martin J. Siebert<sup>7</sup> 

<sup>1</sup>Center for Neutrino Physics, Department of Physics, Virginia Tech, Blacksburg, VA 24061, USA; <sup>2</sup>Department of Physics and Astronomy, University of California, Los Angeles, CA 90095-1547, USA; <sup>3</sup>Kavli Institute for the Physics and Mathematics of the Universe (WPI), UTIAS, The University of Tokyo, Kashiwa, Chiba 277-8583, Japan; <sup>4</sup>Institute for Marine and Atmospheric Research, Utrecht University, Utrecht, The Netherlands; <sup>5</sup>Jet Propulsion Laboratory, California Institute of Technology, Pasadena, CA 91109 USA; <sup>6</sup>Departments of Geophysics and Electrical Engineering, Stanford University, Stanford, CA, USA and <sup>7</sup>Grantham Institute and Department of Earth Science and Engineering, Imperial College London, South Kensington, London SW7 2AZ, UK

**Abstract**

The Antarctic Impulsive Transient Antenna (ANITA) balloon experiment was designed to detect radio signals initiated by high-energy neutrinos and cosmic ray (CR) air showers. These signals are typically discriminated by the polarization and phase inversions of the radio signal. The reflected signal from CRs suffer phase inversion compared to a direct ‘tau neutrino’ event. In this paper, we study subsurface reflection, which can occur without phase inversion, in the context of the two anomalous up-going events reported by ANITA. It is found that subsurface layers and firn density inversions may plausibly account for the events, while ice fabric layers and wind ablation crusts could also play a role. This hypothesis can be tested with radar surveying of the Antarctic region in the vicinity of the anomalous ANITA events. Future experiments should not use phase inversion as a sole criterion to discriminate between down-going and up-going events, unless the subsurface reflection properties are well understood.

**1. Introduction**

Cosmic ray (CR) protons and nuclei bombard the Earth at a wide range of energies. The highest energy CR are thought to originate outside of the Milky Way, and given the extreme distances traveled will have a high probability to scatter on the ubiquitous Big Bang relic radiation dubbed the Cosmic Microwave Background (CMB). This proton–photon scattering process is predicted to produce a flux of neutrinos at the EeV ( $10^{18}$  eV) scale.

The Antarctic Impulsive Transient Antenna (ANITA) experiment searches for neutrinos at the EeV scale using an array of radio antennas attached to a helium balloon that flies over Antarctica at 37 km altitude. The incoming EeV scale neutrinos produce a characteristic radio signal via the Askaryan effect. If ANITA were to find such neutrinos, the experiment should only observe them at shallow angles, such that the neutrino does not intersect much of the Earth or ice. This is due to the fact that neutrinos, although weakly-interacting, suffer severe attenuation through the Earth at these energies.

This makes the recent observation by the ANITA experiment of two steeply pointed up-going events with energies near the EeV ( $10^{18}$  eV) scale very mysterious (Gorham, 2016, 2018). For reference, see Fig. 1 for the location of the two observed ANITA events. While neutrino interactions at high energies are uncertain (Kusenko and Weiler, 2002), the observed events would require neutrino fluxes well in excess of upper limits from Pierre Auger Observatory (Aab and others, 2015) and IceCube (Aartsen, 2016; Romero-Wolf, 2019). A number of new physics explanations for the anomaly have been proposed (Cherry and Shoemaker, 2019; Anchordoqui and others, 2018; Huang, 2018; Dudas and others, 2018; Collins and others, 2019; Chauhan and Mohanty, 2019; Anchordoqui and Antoniadis, 2019; Heurtier and others, 2019; Hooper and others, 2019; Cline and others, 2019).

In addition to neutrino searches, ANITA is also sensitive to CR, finding ~30 such events (Gorham, 2016, 2018; Hoover, 2010). When a CR hits the atmosphere, they produce extensive air showers (EAS) consisting of energetic charged particles which create a characteristic radio signal. Most of the CR events appearing to originate from the Earth display a characteristic phase reversal consistent with the interpretation that the signal originated from a down-going CR-initiated EAS reflected by the Antarctic surface. However, the two anomalous up-going EASs reported by ANITA (Gorham, 2016, 2018) lack phase inversion, and they appear to be inconsistent with such surface reflections. Thus, the phase reversal from ice reflection is the critical observational discriminant between neutrino and CR events.

In this paper, we consider the possibility that the mysterious events are explained by the radio signals originating from down-going CR-initiated EAS reflected by subsurface features in the Antarctic ice which allow for reflections without a phase inversion. Phase inversion occurs when the radio waves traveling in a medium with a low index of refraction (air) reflect

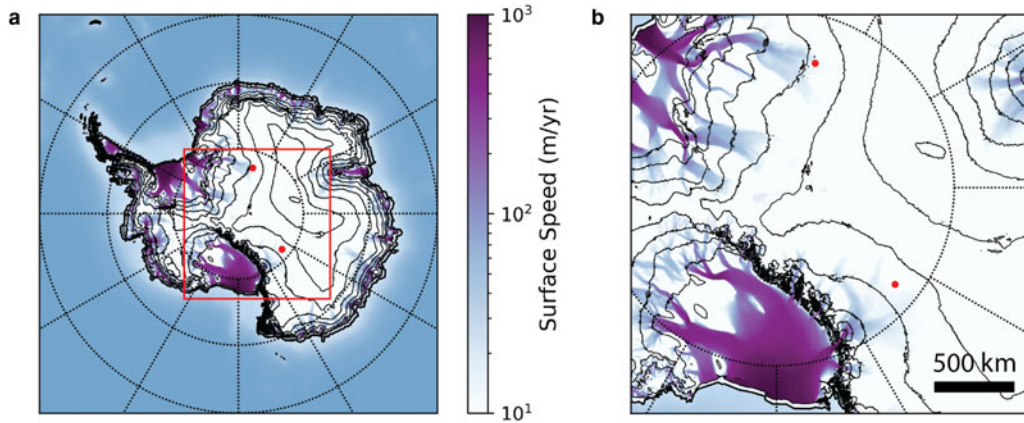


**Fig. 1.** A map (Panel A) and zoom-in (Panel B) of Antarctica displaying the two anomalous upward-pointing events (red dots) observed by the ANITA experiment, overlaid with surface ice speed (purple/blue heat map) and 500 m surface elevation contours. Event 3985267 (upper red dot) was originally reported in Gorham (2016), while event 15717147 (lower red dot) was reported in Gorham (2018). The surface ice speed data come from Mougnot and others (2019) and the surface elevation data come from Morlighem (2019). Both ANITA events lie in low surface ice-speed and high-elevation (3000–3500 m) regions.

from an interface with a medium that has a high index of refraction (ice). Note that higher density ice has a higher index of refraction due to the fact that higher density ice has a lowered speed of electromagnetic wave propagation. Note further that the continuity of electric and magnetic fields across the interface implies that the phase inversion occurs for low-to-high index reflection, but not for high-to-low index reflection. Thus, if the reflection occurs from an interface of a high-density layer on top and a low-density layer on the bottom, there is no phase inversion. We will identify the properties of the Antarctic ice that are required for the radio signal from an ordinary CR air shower to undergo a reflection without a phase inversion, and we will also identify the features known to exist in Antarctic ice that can be responsible for such reflections capable to explain the ANITA events.

**2. General features of subsurface reflectors**

ANITA reports 33 events with phases consistent with the expectations from CR-induced EAS events (Gorham, 2016, 2018; Hoover, 2010; Allison and others, 2018). We compute the number of events above detection threshold  $E_{thr}$  in an observing time,  $T$ , reflecting from either surface or subsurface features with area coverage,  $A_{eff}$ , as

$$N \simeq A_{eff} T \times \int_{E_{thr}}^{\infty} \Phi(E) dE$$

$$= A_{eff} T \times \frac{\Phi_0}{(\gamma - 1)E_0} \left(\frac{E_{thr}}{E_0}\right)^{1-\gamma}, \tag{1}$$

where we take the CR flux to be a power-law,  $\Phi(E) \simeq \Phi_0(E/E_0)^{-\gamma}$  with  $\gamma \simeq 2.7$  (Blasi, 2013). This allows us to estimate the total number of ordinary EAS events from the surface reflection (with phase inversion):

$$N_{CR} \simeq A_{eff} T \times R_{surf.} \times \alpha_{CR}, \tag{2}$$

where we define  $\alpha_{CR} \equiv \Phi_0/(\gamma - 1) E_0 \sim (E_{thr}/E_0)^{1-\gamma}$ ,  $R_{surf.}$  is the surface reflection coefficient, and  $A_{eff}$  is the effective area surveyed by ANITA in flight time  $T$ .

Similarly, we can estimate the anomalous uninverted radio events from subsurface reflection of CR-induced events. Recall that such events would be labeled by ANITA as ‘up-going’ based on their lack of phase reversal. The subsurface reflections

may occur only for incidence angles small enough, so that the power transmitted into the ice at the air–ice interface is significant. For the firn index of refraction, the power transmitted downward exceeds 80% if the incidence angle is less than 70°. We note that the incident angles of the anomalous ANITA events are well below this upper bound and, in fact, these angles are smaller than the average incidence angle of the CR events (Schoorlemmer, 2016). Therefore, one can estimate the rate of anomalous events as

$$N_{anom.} \simeq \delta A_{eff} T \times (1 - R_{surf.})^2 R_{sub.} \times \alpha_{CR} \tag{3}$$

where  $R_{sub.}$  is the subsurface reflection coefficient, and  $\delta A_{eff}$  is the area of the reflecting subsurface. A priori, there is no reason to assume that  $\delta A_{eff}$  is small. In general,  $\delta A_{eff}$  could exceed  $A_{eff}$ , especially if several layers at different depths are contributing to the subsurface reflections. However, to explain the ANITA events, only a small fraction of ice needs to host the reflecting features. The estimates in Eqs. (2) and (3) imply that the subsurface features should occupy an area

$$\left(\frac{\delta A_{eff}}{A_{eff}}\right) \simeq \frac{R_{surf.}}{(1 - R_{surf.})^2 R_{sub.}} \left(\frac{N_{anom.}}{N_{CR}}\right), \tag{4}$$

where in order to account for ANITA’s observations one needs,  $N_{CR} = 33$  and  $N_{anom.} = 2$ . We plot the requisite area estimate from Eq. (4) in Fig. 2 as a function of the subsurface index of refraction assuming that the top layer has  $n = 1.3$  (Kravchenko and others, 2004). See the Appendix for a more detailed discussion of the assumptions going into this calculation.

In summary, a relevant candidate subsurface feature needs to satisfy the following requirements:

1. In accordance with the estimate in Fig. 2,  $\geq 7\%$  of the area should host a reflector at some depth.
2. There should not be significant attenuation for the EAS radio pulse above the reflecting feature, since this would render the signal undetectable. Roughly, if the detected anomalous event was attenuated by  $\leq 0.2$ , the resulting field amplitude would drop below the trigger threshold (Romero-Wolf, 2019). Since the attenuation length for radio waves in ice is 1.2–1.5 km (with some temperature dependence (Matsuoka and others, 2012)) for the frequencies probed by ANITA, this requirement is satisfied by any features not obstructed by an overlying layer of liquid water (the attenuation length in liquid water is much shorter (Ray, 1972)).

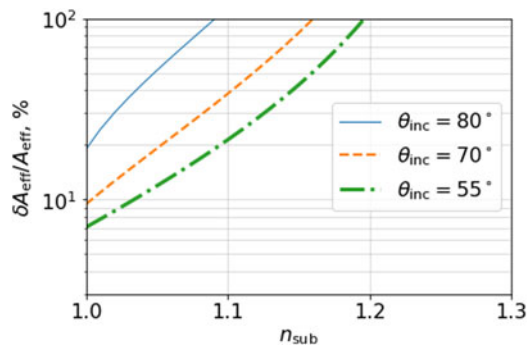


**Fig. 2.** For a two-layer model, we plot the required area coverage of a subsurface reflector as a function of the subsurface index of refraction,  $n_{\text{sub}}$ . Three incidence angles (incidence angle is defined as  $\theta_{\text{inc}} = 180 - \theta_z$ , where  $\theta_z$  is the zenith angle) are shown: incident angles of  $55^\circ$  (roughly corresponding to the anomalous event (Gorham, 2018)),  $70^\circ$  (roughly the average angle for ANITA CRs) and  $80^\circ$  (which is on the high end of incident angles for the ANITA CR events). Here it is assumed that the surface has  $n = 1.3$ .

3. The reflection must occur without a phase inversion. A subsurface interface with a higher index of refraction above and a lower index of refraction below can reflect a signal without a phase inversion. Likewise, multiple layers of variable index of refraction can reflect a signal without a phase shift (Tikhonravov and others, 1997).
4. Given the wavelengths ANITA is sensitive to, the subsurface layer above the reflecting interface needs to be sufficiently thick, although the layer below the interface can be quite thin (Cavitte and others, 2016). Similarly, the features should be  $> 100$  m in diameter in order to be of the first Fresnel zone radius. Lastly, these surfaces likely need to be tilted with respect to the surface, such that double reflections (coincident surface and subsurface reflections) are rare. Note that the relative tilt can produce total internal reflection and suppress the signal. Given random orientations, one can expect this to occur roughly half the time.

Given these requirements, we now proceed to investigate which glaciological candidates may have the correct distribution and reflective properties.

### 3. Subsurface Antarctic candidates

Subsurface features that may have the right properties to account for the anomalous ANITA events include several possibilities:

- (a) **Double layers:** The work of Arcone and others (2005) finds direct evidence for reflective surfaces without phase inversions. In particular, they find evidence for ‘thin double layers of ice over hoar’ which have reflection without inversion, and conclude that they are ‘extensive’ throughout West Antarctica. They model the observed reflections as high-permittivity ice sitting above low-permittivity hoar. The modeling done indicates that hoar thickness fluctuation is a major driver of the phase of the wavelet. These results were obtained with 400 MHz short pulse radar (ANITA is in the 200–800 MHz range).
- (b) **Firn density inversions:** Ligtenberg and others (2011) and Kuipers Munneke and others (2014) estimate snow and firn density (in the top 100 m of depth) in Antarctica for the period 1979–2017 at a horizontal resolution of  $(27 \times 27)$  km<sup>2</sup> and a temporal resolution of 10–15 days, using a firn model that includes not only compaction, but also firn hydrology including melt, percolation and refreezing. The model has not been evaluated at the two locations of the observed ANITA events.
- (c) **Wind/ablation crusts and Sastrugi:** These are abundant in megadune regions, and may create low-density regions with large grains above higher density snow. Sastrugi are essentially wind eroded snow, which make irregular ridges on the surface (Scambos and others, 2012). Given that these regions have a variety of slopes as well, they naturally help explain the lack of double-reflections (simultaneous surface and subsurface reflections). By some estimates, as much as 11% of the East Antarctic Ice Sheet is covered by the so-called ‘wind glaze’ (Scambos and others, 2012), forming a surface with a polished appearance with nearly zero accumulation due to persistent winds. This could produce both the needed reflection phase and range of angles. Since these wind crusts are denser than typical snow, they would naturally have larger indices of refraction than typical surface snow.
- (d) **Ice fabric layers:** Ice-sheet fabrics are formed as a result of rheology and stress, leading to macroscopic ice crystal alignment. Some fabrics appear to have the right dielectric properties to produce a reflection without phase inversion even without the index of refraction contrasts (Matsuoka and others, 2003). In this case, it is the contrasts in crystal orientation fabric that source strong reflections (Matsuoka and others, 2003). The spatial distribution of ice-sheet fabric is not very well known since ice cores are restricted in number and distribution across Antarctica (Wang and others, 2018).

Although there are minor variations in density due of dependence of densification on temperature following the annual cycle, these variations are quite small, and are not large enough to explain the ANITA observations. However, there are additional firm features not accounted for in this model.

For example, ice core samples show substantial density and permittivity variations. We show as an example in the left panel of Fig. 3 a density profile from the East Antarctic Plateau (Laepplé and others, 2016). These density variations are quite substantial and may constitute a plausible candidate for the ANITA events, and they are rather common in the 500 m area sampled in Laepplé and others (2016).

It is well-known that the constructive interference effects from scattering on a medium consisting of multiple thin layers can produce a large reflection coefficient at some wavelengths (Vinogradov and Zeldovich, 1977) (see also Pirozhkov and Ragozin (2015); Stearns (1989) for generalizations). The ice core sample displayed in Fig. 3 has just this structure, consisting of a number of thin layers with small index of refraction differences. Motivated by this, we display two calculations of the reflection coefficients in Fig. 3. In one case (the red curve), we compute reflection from a medium consisting of regularly spaced layers of 10 cm thickness. This results in a sharp resonance feature, as expected (Vinogradov and Zeldovich, 1977). In contrast, the blue curve assumes layers whose thickness is randomly chosen between 3 and 15 cm. In both instances, the layers have alternating refraction indices, chosen between  $n_1 = 1.3$  and  $n_2 = 1.6$  for a  $60^\circ$  incidence angle. We have explicitly computed the phase change in reflections from regular and random layers, and found that the phase shifts are close to zero for the range of wavelengths with maximal reflectivity, in agreement with the results of Tikhonravov and others (1997) for regular layers. We note that reflections from multiple layers will induce a time delay, impacting the measured time profile of the pulse. This makes a multi-layer reflection interpretation of the event reported in Gorham (2018) unlikely, though it may be a candidate explanation for the event in Gorham (2016). We stress that the specific ice core sample in the left panel of Fig. 3 and the modeled reflection coefficient in the right panel of Fig. 3 are to be understood merely as a proof-of-principle.

- (c) **Wind/ablation crusts and Sastrugi:** These are abundant in megadune regions, and may create low-density regions with large grains above higher density snow. Sastrugi are essentially wind eroded snow, which make irregular ridges on the surface (Scambos and others, 2012). Given that these regions have a variety of slopes as well, they naturally help explain the lack of double-reflections (simultaneous surface and subsurface reflections). By some estimates, as much as 11% of the East Antarctic Ice Sheet is covered by the so-called ‘wind glaze’ (Scambos and others, 2012), forming a surface with a polished appearance with nearly zero accumulation due to persistent winds. This could produce both the needed reflection phase and range of angles. Since these wind crusts are denser than typical snow, they would naturally have larger indices of refraction than typical surface snow.
- (d) **Ice fabric layers:** Ice-sheet fabrics are formed as a result of rheology and stress, leading to macroscopic ice crystal alignment. Some fabrics appear to have the right dielectric properties to produce a reflection without phase inversion even without the index of refraction contrasts (Matsuoka and others, 2003). In this case, it is the contrasts in crystal orientation fabric that source strong reflections (Matsuoka and others, 2003). The spatial distribution of ice-sheet fabric is not very well known since ice cores are restricted in number and distribution across Antarctica (Wang and others, 2018).

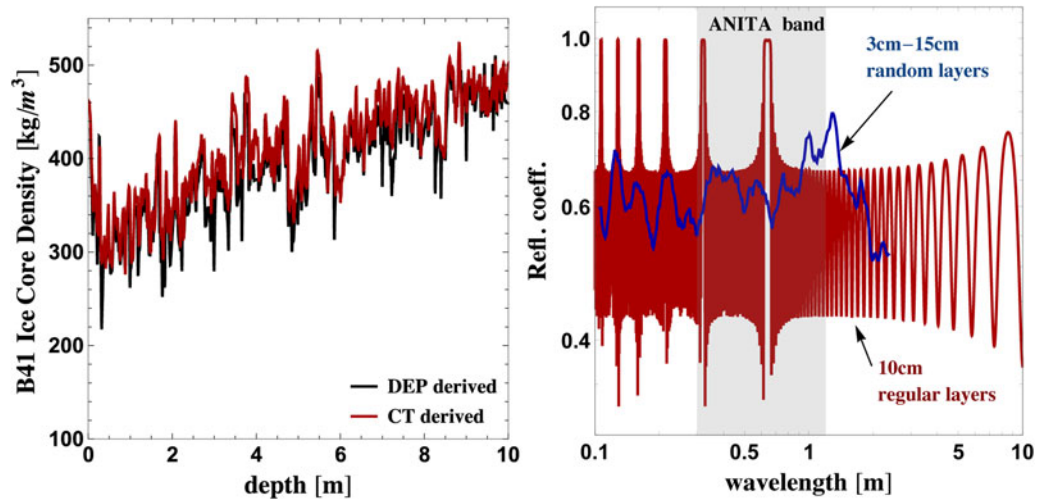


**Fig. 3.** *Left panel:* An example Ice Core sample from the East Antarctic Plateau (Laepple and others, 2016). Here the black curve shows the density from a dielectric profiling (DEP) technique, while the red shows the result from high-resolution X-ray computer tomography (CT). *Right panel:* Power reflection coefficients (in power) for scattering from a multilayered medium as a function of wavelength. The red curve is calculated assuming regularly spaced layers of 10 cm thickness, whereas the blue curve assumes layers whose thickness is randomly chosen between 3 and 15 cm.

There is some indication that ice fabric layers are more widespread than originally believed (Wang and others, 2018; Siegert and Fujita, 2001; Siegert and Kwok, 2000), which makes it plausible that the distribution is sufficiently common to produce the observed reflections.

- (e) **Subglacial lakes:** Most lakes appear to be hydrostatically sealed, and therefore lack an air–water interface which would otherwise provide a useful reflecting surface without phase inversion. The bottom of the lake could in principle work, but only rather shallow and low conductivity subglacial lake regions (Schroeder and others, 2015) would be able to produce a reflection without significant attenuation in water. Exploiting the time delay and amplitude attenuation in water, radio echo surveys provided the first direct evidence for that subglacial lakes were at least several meters deep (Gorman and Siegert, 1999). Recent model estimates suggest that  $(0.6 \pm 0.2)\%$  of the Antarctic ice/bed interface is covered by subglacial lakes (Goeller and others, 2016). Given that subglacial lakes lack a water–air boundary, and that they cover  $<1\%$  of the Antarctic area, we do not consider these especially promising candidates for ANITA. We note however the possibility that impurities in the accreted ice above a lake could in principle produce a higher index of refraction layer above a lower index layer, though is likely uncommon. We note that the ice above Lake Vostok has been found to contain ice fabric contrasts, which could source strong reflections (MacGregor and others, 2009).
- (f) **Snow-covered crevasses/hollow caves/ice bridges:** An ice-to-air boundary would have the correct properties for reflection without phase inversion. However, fumarolic and volcanic ice caves do not seem to be sufficiently common for the ANITA events. Crevasses are common in regions of fast flow, but are not common in the middle of the ice sheet where the ANITA events are observed. Note however that drained subglacial lakes (e.g. dolines) are more widespread than previously, and thereby present an additional mechanism for the generation of air cavities within the ice (Lenaerts and others, 2017).
- (g) **Englacial layers of dielectric and/or density contrasts:** At depths beyond the firn (though still  $\leq 1$  km), dielectric contrasts in the ice may be sufficiently common to explain the events (Peters and others, 2005; Barnes and others, 2006). Moreover, in principle, density contrasts in deep englacial

layers qualitatively similar to what is displayed in Fig. 3 may also source strong reflection coefficients. Recently, radar has been used to detect layers of sediment within the ice (Winter and others, 2019), which could also form a strong englacial dielectric.

#### 4. Future probes

We summarize the status of potential candidates in Table I. Future probes of subsurface reflections can be designed to definitively test the origin of ANITA events and to learn about the properties of Antarctic ice. One can identify the subsurface structures causing reflections by following up with a radar observation at the sites of anomalous events. Although this capability does not yet exist, it may be possible to design a future ANITA-like neutrino experiment using two spatially separated detectors for simultaneous observations of the same reflection, which could provide additional information about the subsurface layers. We leave a dedicated analysis of these possibilities for future work.

If subsurface features are ultimately responsible for the ANITA events, the distribution and extent of such features will be important for ANITA going forward. Moreover, a dedicated effort to determine if the ANITA events originate from a subsurface reflector may be relevant for glaciology by providing additional information such as the extent, spatial distribution and reflective properties of these features.

In addition, it is possible that ANITA's ultra-high-energy CR waveforms may contain signs (or telling absences) of sub-surface reflections, which may produce multiple or spatially overlapping pulses. Such overlapping pulses can be expected to occur when both surface and sub-surface reflection occurs from the same originating event. Although the two up-going ANITA events do not show evidence of pulse overlap, future data may help elucidate the viability of this hypothesis if overlapping pulses are observed.

Moreover, there are additional relevant data sets that can be exploited in order to provide a comprehensive understanding of surface and sub-surface reflection characteristics. For example, digital echo models (with near total continental coverage) could be utilized for a surface roughness analysis for possible phase inversion (Howat and others, 2019). Second, The Center for Remote Sensing of Ice Sheets (CREGIS) has used ultra-wideband microwave radar to map near-surface internal layers in polar

**Table 1.** Summary table of candidates and their ability to satisfy the requirements of the ANITA observations

	>7% Area coverage	Reflection without inversion	>100 m diameter
Double layers	✓	✓	✓
Firn density inversions	✓	✓	✓
Wind crusts	?	✓	✓
Ice fabrics	?	✓	✓
Subglacial lakes	X	✓	✓
Air pockets	X	✓	✓

firn, which may contain information on near surface (<1 m depths) reflections (Panzer and others, 2013). Further, the High-Altitude Calibration (HiCal) instrument collected data which specifically targeted surface reflection characteristics (Gorham, 2019).

Additional candidates may come from subsurface features originating from pond refreezing although these may only be limited to ice shelves (Hubbard, 2016).

## 5. Conclusions

This paper has examined the possibility of the anomalous up-going ANITA events as originating from ordinary CR-initiated air showers. For this to be consistent with the phase information ANITA observes, they must reflect from a subsurface feature without phase inversion. We have investigated a number of glaciological candidates in order to determine which of these may have properties consistent with ANITA's observations. We have found that subsurface double layers and firn density inversions are a plausible explanation of the anomalous events. In order to conclusively test if surface/subsurface glaciological candidates are responsible for the ANITA events, more information is needed on candidate location, fraction of occurrence in the area sampled by ANITA and a more detailed analysis of the ANITA acceptance. We note that, while firn density contrasts appear to be a plausible candidate, one or more of the other glaciological features discussed here may play a sub-dominant role in sourcing strong un-inverted reflections.

Our results have broad implications for future neutrino and CR experiments. Given the possibility of reflections without a phase inversion, future experiments should not use the phase inversion in radio signals as a sole criterion for discriminating between down-going and up-going events, unless the properties of the subsurface reflection are well understood.

**Acknowledgments.** We thank the useful feedback from our anonymous reviewers and our Scientific Editor Olaf Eisen. We are very grateful to Thomas Laepple for providing the B41 ice core data from Ref. (Laepple and others, 2016). Furthermore, we acknowledge helpful discussions with Kumiko Azuma, Dmitry Chirkin, Francis Halzen, Stefan Ligtenberg, Henning Loewe and David Saltzberg. The work of I.M.S. is supported by the US Department of Energy under the award number DE-SC0020250. The work of A.K. was supported by the US Department of Energy Grant No. DE-SC0009937, and by the World Premier International Research Center Initiative (WPI), MEXT, Japan. Part of this work was carried out at the Jet Propulsion Laboratory, California Institute of Technology, under a contract with the National Aeronautics and Space Administration. P.K.M. is supported by the Netherlands Earth System Science Centre (NESSC).

## References

**Aab A and 42 others** (2015) Improved limit to the diffuse flux of ultrahigh energy neutrinos from the Pierre Auger Observatory. *Physical Review D* **91**(9), 092008. doi: [10.1103/PhysRevD.91.092008](https://doi.org/10.1103/PhysRevD.91.092008).

- Aartsen MG and 309 others** (2016) Constraints on Ultrahigh-Energy Cosmic-Ray Sources from a Search for Neutrinos above 10 PeV with IceCube. *Physical Review Letters* **117**(24), 241101. doi: [10.1103/PhysRevLett.117.241101](https://doi.org/10.1103/PhysRevLett.117.241101). [Erratum: Phys. Rev. Lett.119,no.25,259902 (2017)].
- Allison P and 59 others** (2018) Constraints on the diffuse high-energy neutrino flux from the third flight of ANITA. *Physical Review D* **98**(2), 022001. doi: [10.1103/PhysRevD.98.022001](https://doi.org/10.1103/PhysRevD.98.022001).
- Anchordoqui LA and Antoniadis I** (2019) Supersymmetric sphaleron configurations as the origin of the perplexing ANITA events. *Physics Letters B* **790**, 578–582. doi: [10.1016/j.physletb.2019.02.003](https://doi.org/10.1016/j.physletb.2019.02.003).
- Anchordoqui LA, Barger V, Learned JG, Marfatia D and Weiler TJ** (2018) Upgoing ANITA events as evidence of the CPT symmetric universe. *Letters in High Energy Physics* **1**(1), 13–16. doi: [10.31526/LHEP.1.2018.03](https://doi.org/10.31526/LHEP.1.2018.03).
- Arcone SA, Spikes VB and Hamilton GS** (2005) Phase structure of radar stratigraphic horizons within Antarctic firn. *Annals of Glaciology* **41**, 10–16. doi: [10.3189/172756405781813267](https://doi.org/10.3189/172756405781813267).
- Barnes PRF, Wolff EW and Mulvaney R** (2006) A 44 kyr paleoroughness record of the Antarctic surface. *Journal of Geophysical Research: Atmospheres* **111**, 1–11 (D3). doi: [10.1029/2005JD006349](https://doi.org/10.1029/2005JD006349).
- Blasi P** (2013) The Origin of Galactic Cosmic Rays. *The Astronomy and Astrophysics Review* **21**, 70. doi: [10.1007/s00159-013-0070-7](https://doi.org/10.1007/s00159-013-0070-7).
- Cavitt MGP and 7 others** (2016) Deep radiostratigraphy of the East Antarctic plateau: connecting the Dome C and Vostok ice core sites. *Journal of Glaciology* **62**(232), 323–334. doi: [10.1017/jog.2016.11](https://doi.org/10.1017/jog.2016.11).
- Chauhan B and Mohanty S** (2019) A common leptoquark solution of flavor and ANITA anomalies. *Physical Review D* **99**(9), 095018. doi: [10.1103/PhysRevD.99.095018](https://doi.org/10.1103/PhysRevD.99.095018).
- Cherry JF and Shoemaker IM** (2019) Sterile neutrino origin for the upward directed cosmic ray showers detected by ANITA. *Physical Review D* **99**(6), 063016. doi: [10.1103/PhysRevD.99.063016](https://doi.org/10.1103/PhysRevD.99.063016).
- Cline JM, Gross C and Xue W** (2019) Can the ANITA anomalous events be due to new physics?. *Physical Review D* **100**(1), 015031. doi: [10.1103/PhysRevD.100.015031](https://doi.org/10.1103/PhysRevD.100.015031).
- Collins JH, Bhupal Dev PS and Sui Y** (2019) R-parity Violating Supersymmetric Explanation of the Anomalous Events at ANITA. *Physical Review D* **99**(4), 043009. doi: [10.1103/PhysRevD.99.043009](https://doi.org/10.1103/PhysRevD.99.043009).
- Dudas E, Gherghetta T, Kaneta K, Mambrini Y and Olive KA** (2018) Gravitino decay in high scale supersymmetry with R -parity violation. *Physical Review D* **98**(1), 015030. doi: [10.1103/PhysRevD.98.015030](https://doi.org/10.1103/PhysRevD.98.015030).
- Goeller S, Steinhage D, Thoma M and Grosfeld K** (2016) Assessing the subglacial lake coverage of Antarctica. *Annals of Glaciology* **57**(72), 109–117. doi: [10.1017/aog.2016.23](https://doi.org/10.1017/aog.2016.23).
- Gorham PW and 68 others** (2016) Characteristics of Four Upward-pointing Cosmic-ray-like Events Observed with ANITA. *Physical Review Letters* **117**(7), 071101. doi: [10.1103/PhysRevLett.117.071101](https://doi.org/10.1103/PhysRevLett.117.071101).
- Gorham PW and 62 others** (2018) Observation of an Unusual Upward-going Cosmic-ray-like Event in the Third Flight of ANITA. *Physical Review Letters* **121**(16), 161102. doi: [10.1103/PhysRevLett.121.161102](https://doi.org/10.1103/PhysRevLett.121.161102).
- Gorham PW and 57 others** (2019) HiCal 2: An instrument designed for calibration of the ANITA experiment and for Antarctic surface reflectivity measurements. *Nuclear Instruments and Methods in Physics A* **918**, 60–66. doi: [10.1016/j.nima.2018.11.092](https://doi.org/10.1016/j.nima.2018.11.092).
- Gorman MR and Siegert MJ** (1999) Penetration of Antarctic subglacial lakes by VHF electromagnetic pulses: Information on the depth and electrical conductivity of basal water bodies. *Journal of Geophysical Research: Solid Earth* **104**(B12), 29311–29320. doi: [10.1029/1999JB900271](https://doi.org/10.1029/1999JB900271).
- Heurtier L, Mambrini Y and Pierre M** (2019) A Dark Matter Interpretation of the ANITA Anomalous Events. *Physical Review D* **99**(9), 095014. doi: [10.1103/PhysRevD.99.095014](https://doi.org/10.1103/PhysRevD.99.095014).
- Hooper D, Wegsman S, Deaconu C and Vieregge A** (2019) Superheavy Dark Matter and ANITA's Anomalous Events. *Physical Review D* **100**(4), 043019. doi: [10.1103/PhysRevD.100.043019](https://doi.org/10.1103/PhysRevD.100.043019).
- Hoover S and 47 others** (2010) Observation of Ultrahigh-Energy Cosmic Rays with the ANITA Balloon-Borne Radio Interferometer. *Physical Review Letters* **105**(15), 151101. doi: [10.1103/PhysRevLett.105.151101](https://doi.org/10.1103/PhysRevLett.105.151101).
- Howat IM, Porter C, Smith BE, Noh MJ and Morin P** (2019) The reference elevation model of antarctica. *The Cryosphere* **13**(2), 665–674. doi: [10.5194/tc-13-665-2019](https://doi.org/10.5194/tc-13-665-2019).
- Huang Gy** (2018) Sterile neutrinos as a possible explanation for the upward air shower events at ANITA. *Physical Review D* **98**(4), 043019. doi: [10.1103/PhysRevD.98.043019](https://doi.org/10.1103/PhysRevD.98.043019).

- Hubbard B and 12 others** (2016) Massive subsurface ice formed by refreezing of ice-shelf melt ponds. *Nature communications* **7**, 11897. doi: [10.1038/ncomms11897](https://doi.org/10.1038/ncomms11897).
- Kravchenko I, Besson D and Meyers J** (2004) In situ index-of-refraction measurements of the south polar firn with the rice detector. *Journal of Glaciology* **50**(171), 522–532. doi: [10.3189/172756504781829800](https://doi.org/10.3189/172756504781829800).
- Kuipers Munneke P, Ligtenberg SR, van den Broeke MR and Vaughan DG** (2014) Firn air depletion as a precursor of Antarctic ice-shelf collapse. *Journal of Glaciology* **60**(220), 205–214. doi: [10.3189/2014JoG13J183](https://doi.org/10.3189/2014JoG13J183).
- Kusenko A and Weiler TJ** (2002) Neutrino cross-sections at high-energies and the future observations of ultrahigh-energy cosmic rays. *Physical Review Letters* **88**, 161101. doi: [10.1103/PhysRevLett.88.161101](https://doi.org/10.1103/PhysRevLett.88.161101).
- Laepple T and 5 others** (2016) Layering of surface snow and firn at Kohlen Station, Antarctica: Noise or seasonal signal?. *Journal of Geophysical Research: Earth Surface* **121**(10), 1849–1860. doi: [10.1002/2016JF003919](https://doi.org/10.1002/2016JF003919).
- Lenaerts JTM and 12 others** (2017) Meltwater produced by wind-albedo interaction stored in an east antarctic ice shelf. *Nature Climate Change* **7**, 58–63. doi: [10.1038/NCLIMATE3180](https://doi.org/10.1038/NCLIMATE3180).
- Ligtenberg SRM, Helsen MM, van den Broeke MR** (2011) An improved semi-empirical model for the densification of Antarctic firn. *The Cryosphere* **5**(4), 809–819. doi: [10.5194/tc-5-809-2011](https://doi.org/10.5194/tc-5-809-2011).
- MacGregor J, Matsuoka K and Studinger M** (2009) Radar detection of accreted ice over Lake Vostok, Antarctica. *Earth and Planetary Science Letters* **282**(1), 222–233. doi: [10.1016/j.epsl.2009.03.018](https://doi.org/10.1016/j.epsl.2009.03.018).
- Matsuoka K and 6 others** (2003) Crystal orientation fabrics within the Antarctic ice sheet revealed by a multipolarization plane and dual-frequency radar survey. *Journal of Geophysical Research: Solid Earth* **108**(B10), 1–17. doi: [10.1029/2003JB002425](https://doi.org/10.1029/2003JB002425).
- Matsuoka K, MacGregor JA and Pattyn F** (2012) Predicting radar attenuation within the Antarctic ice sheet. *Earth and Planetary Science Letters* **359**, 173–183. doi: [10.1016/j.epsl.2012.10.018](https://doi.org/10.1016/j.epsl.2012.10.018).
- Morlighem M and 37 others** (2019) Deep glacial troughs and stabilizing ridges unveiled beneath the margins of the Antarctic ice sheet. *Nature Geoscience* **13**, 132–137. doi: [10.1038/s41561-019-0510-8](https://doi.org/10.1038/s41561-019-0510-8).
- Mouginot J, Rignot E and Scheuchl B** (2019) Continent-wide, interferometric SAR phase, mapping of antarctic ice velocity. *Geophysical Research Letters* **46**(16), 9710–9718. doi: [10.1029/2019GL083826](https://doi.org/10.1029/2019GL083826).
- Panzer B and 8 others** (2013) An ultra-wideband, microwave radar for measuring snow thickness on sea ice and mapping near-surface internal layers in polar firn. *Journal of Glaciology* **59**(214), 244–254. doi: [10.3189/2013JoG12J128](https://doi.org/10.3189/2013JoG12J128).
- Peters ME, Blankenship DD and Morse DL** (2005) Analysis techniques for coherent airborne radar sounding: Application to West Antarctic ice streams. *Journal of Geophysical Research: Solid Earth* **110**(B6). doi: [10.1029/2004JB003222](https://doi.org/10.1029/2004JB003222).
- Pirozhkov AS and Ragozin EN** (2015) Aperiodic multilayer structures in soft X-ray optics. *Physics Uspekhi (Advances in Physical Sciences)* **58**(11), 1095–1105. doi: [10.3367/ufne.0185.201511e.1203](https://doi.org/10.3367/ufne.0185.201511e.1203).
- Ray PS** (1972) Broadband complex refractive indices of ice and water. *Applied Optics* **11**(8), 1836–1844. doi: [10.1364/AO.11.001836](https://doi.org/10.1364/AO.11.001836).
- Romero-Wolf A and 56 others** (2019) A comprehensive analysis of anomalous ANITA events disfavors a diffuse tau-neutrino flux origin. *Physical Review D* **99**(6), 063011. doi: [10.1103/PhysRevD.99.063011](https://doi.org/10.1103/PhysRevD.99.063011).
- Scambos TA and 12 others** (2012) Extent of low-accumulation ‘wind glaze’ areas on the East Antarctic plateau: implications for continental ice mass balance. *Journal of Glaciology* **58**, 633–647. doi: [10.3189/2012JoG11J232](https://doi.org/10.3189/2012JoG11J232).
- Schoorlemmer H and 66 others** (2016) Energy and flux measurements of ultra-high energy cosmic rays observed during the first ANITA flight. *Astroparticle Physics* **77**, 32–43. doi: [10.1016/j.astropartphys.2016.01.001](https://doi.org/10.1016/j.astropartphys.2016.01.001).
- Schroeder DM, Blankenship DD, Raney RK and Grima C** (2015) Estimating subglacial water geometry using radar bed echo specularity: Application to Thwaites Glacier, West Antarctica. *IEEE Geoscience and Remote Sensing Letters* **12**, 443–447. doi: [10.1109/LGRS.2014.2337878](https://doi.org/10.1109/LGRS.2014.2337878).
- Siebert MJ and Fujita S** (2001) Internal ice-sheet radar layer profiles and their relation to reflection mechanisms between Dome C and the Transantarctic Mountains. *Journal of Glaciology* **47**(157), 205–212. doi: [10.3189/172756501781832205](https://doi.org/10.3189/172756501781832205).
- Siebert MJ and Kwok R** (2000) Ice-sheet radar layering and the development of preferred crystal orientation fabrics between Lake Vostok and Ridge B, central East Antarctica. *Earth and Planetary Science Letters* **179**(2), 227–235. doi: [10.1016/S0012-821X\(00\)00121-7](https://doi.org/10.1016/S0012-821X(00)00121-7).
- Stearns DG** (1989) The scattering of X-rays from nonideal multilayer structures. *Journal of Applied Physics* **65**(2), 491–506. doi: [10.1063/1.343131](https://doi.org/10.1063/1.343131).
- Tikhonravov AV, Baumeister PW and Popov KV** (1997) Phase properties of multilayers. *Applied Optics* **36**(19), 4382–4392. doi: [10.1364/AO.36.004382](https://doi.org/10.1364/AO.36.004382).
- Vinogradov AV and Zeldovich BY** (1977) X-ray and far UV multilayer mirrors: Principles and possibilities. *Applied Optics* **16**, 89–93. doi: [10.1364/AO.16.000089](https://doi.org/10.1364/AO.16.000089).
- Wang B and 6 others** (2018) Summit of the East Antarctic Ice Sheet underlain by thick ice-crystal fabric layers linked to glacial-interglacial environmental change. *Geological Society of London Special Publications* **461**, 131–143. doi: [10.1144/SP461.1](https://doi.org/10.1144/SP461.1).
- Winter Kate, Woodward John, Ross Neil, Dunning Stuart A., Hein Andrew S., Westoby Matthew J., Culberg Riley, Marrero Shasta M., Schroeder Dustin M., Sugden David E. and Siegert Martin J.** (2019) Radar-Detected Englacial Debris in the West Antarctic Ice Sheet. *Geophysical Research Letters* **46**(17-18), 10454–10462. doi: [http://dx.doi.org/10.1029/2019GL084012](https://doi.org/10.1029/2019GL084012).

## Appendix: Acceptance of reflected cosmic rays

The number of events detected due to an isotropic flux  $\phi(E)$ , integrated over a band of energies  $E$ , flowing through a reference area  $A$  and a range of directions given by solid angle  $\Omega$ , depends on the observation time  $t$  and detection efficiency  $P_{\text{det}}$ , which, in general, are dependent on all the variables of integration.

$$N = \int_0^{\infty} dE \int_0^T dt \int_A dA \int_{\Omega} d\Omega (\hat{r} \cdot \hat{n}) P_{\text{det}} \phi(E). \quad (1)$$

Evaluating this integral for an experiment accurately is an involved calculation requiring Monte Carlo simulations and detailed instrument response model. For the purposes of this study, we seek only to bound the behavior of subsurface reflection cosmic ray events in relation to the surface reflection events. For a radio detector, the air shower geometry can be described by taking a point on the surface of the Earth ( $A$ ) and a direction within solid angle  $\Omega$ . Since the cosmic ray flux is predominantly isotropic, the range of angles is uniform in the sky. The cosmic ray air shower produces an electric field  $\mathcal{E}$  with amplitude proportional to its energy  $E$ . The electric field is reflected off the ice and induces a voltage  $V$  at the antenna terminals. A simple model of the detection probability  $P_{\text{det}}$  is that the voltage  $V$  exceeds a threshold value  $V_{\text{thr}}$  so that  $P_{\text{det}} \propto \Theta(V - V_{\text{thr}})$ , where  $\Theta$  is the Heaviside step function. The voltage is related to the electric field  $\mathcal{E}$  via  $V = h\mathcal{E}$  where  $h$  is the effective length of the antenna, which is direction and frequency dependent.

The zeroth-order approximation is to take a characteristic value of the effective length  $h \simeq h_0$  for the range of frequencies and directions relevant to ANITA. In this case, we can translate  $P_{\text{det}} \simeq \Theta(\mathcal{E} - \mathcal{E}_{\text{thr}})$  and  $\mathcal{E}_{\text{thr}} = V_{\text{thr}}/h_0$ .

The electric field is related to the energy of the cosmic ray air shower via  $\mathcal{E} \simeq \mathcal{E}_0 \alpha (E/E_0) (d_0/d)$  where  $E_0$  is a reference energy,  $d$  is the distance to shower maximum along the reflection path,  $d_0$  is a reference distance, and  $\mathcal{E}_0$  is a proportionality constant. We have omitted the relation of the magnetic field (mostly vertical in Antarctica) to the direction of the shower and assume an average value here. The value  $\alpha$  here is meant to capture the effects of reflections and transmission through ice for the various cases under consideration. To zeroth order, we omit the dependence on cosmic ray direction and approximate the distance to the cosmic ray shower maximum as  $d \simeq d_0$  so that  $\mathcal{E} \simeq \mathcal{E}_0 \alpha (E/E_0)$ . With this approximation, we can assume a threshold energy  $E_{\text{thr}} = E_0 (\mathcal{E}_{\text{thr}}/\mathcal{E}_0)/\alpha$ .

The cosmic ray flux, over a limited energy band, can be approximated by a power law  $\phi(E) \simeq \phi_0 (E/E_0)^{-\gamma}$ . With our zeroth-order approximations on the direction of cosmic rays

$$N \simeq T \langle A\Omega \rangle_0 \phi_0 \int_{E_{\text{thr}}}^{\infty} dE (E/E_0)^{-\gamma} \quad (2)$$

where the acceptance  $\langle A\Omega \rangle$  is the combination of points on the surface and cosmic ray arrival directions that would trigger the detector given by

$$\langle A\Omega \rangle = \int_A dA \int_{\Omega} d\Omega (\hat{r} \cdot \hat{n}) P_{\text{det}} \quad (3)$$

This value is generally energy dependent but in our zeroth-order

approximation, we are evaluating  $\langle A\Omega \rangle_0$  at a characteristic energy  $E_0$ . With our approximations, we arrive at

$$N \simeq T \frac{\langle A\Omega \rangle_0 \phi_0}{(\gamma - 1)E_0} \left( \frac{E_{\text{thr}}}{E_0} \right)^{1-\gamma} \quad (4)$$

or, in terms of the electric field threshold,

$$N \simeq T \frac{\langle A\Omega \rangle_0 \phi_0}{(\gamma - 1)E_0} \left( \frac{1}{\alpha} \frac{\mathcal{E}_{\text{thr}}}{\mathcal{E}_0} \right)^{1-\gamma}. \quad (5)$$

Now take  $N_{\text{CR}}$  for the surface-reflected cosmic ray events and  $N_{\text{anom}}$  for the anomalous events. Since the hypothesis is that the difference is due to surface reflections and subsurface reflections, we can estimate  $\alpha_{\text{CR}} \simeq r_{\text{refl}}$  where  $r_{\text{refl}}$  is the electric field reflection coefficient of the surface of the ice. For the

subsurface events  $\alpha_{\text{anom}} = (1 - r_{\text{refl}}^2)r_{\text{sub}}$  where  $r_{\text{sub}}$  is the electric field reflection coefficient for the subsurface interface and the factor of  $(1 - r_{\text{refl}}^2)$  is due to the electric field being transmitted in and out of the ice-air interface.

Assuming that the typical direction of surface and subsurface reflected events is comparable (to zeroth order), then we arrive at the ratio

$$\frac{\langle A\Omega \rangle_{\text{anom}}}{\langle A\Omega \rangle_{\text{CR}}} \simeq \frac{N_{\text{anom}}}{N_{\text{CR}}} \left( \frac{r_{\text{refl}}}{(1 - r_{\text{refl}}^2)r_{\text{sub}}} \right)^{\gamma-1} \quad (6)$$

Assuming a spectral index  $\gamma \simeq 3$  and using the power reflection coefficients  $R_{\text{refl}} = r_{\text{refl}}^2$  and  $R_{\text{sub}} = r_{\text{sub}}^2$ , we arrive at the result

$$\frac{\langle A\Omega \rangle_{\text{anom}}}{\langle A\Omega \rangle_{\text{CR}}} \simeq \frac{N_{\text{anom}}}{N_{\text{CR}}} \frac{R_{\text{refl}}}{(1 - R_{\text{refl}})^2 R_{\text{sub}}}. \quad (7)$$